Submitted to Physics Letters B

LBL-4300
Preprint c.1

ANGULAR FOCUSSING IN HEAVILY DAMPED HEAVY ION COLLISIONS

F. Beck

August 1975

Prepared for the U. S. Energy Research and
Development Administration under Contract W-7405-ENG-48

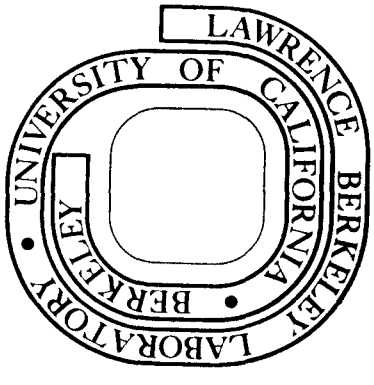

DISCLAIMER

LBL-4300

ANGULAR FOCUSSING IN HEAVILY DAMPED HEAVY ION COLLISIONS*

F. Beck+

Lawrence Berkeley Laboratory
University of California
Berkeley, California 94720

Abstract:

A simple and analytically solvable classical model has been set up to study the influence of various assumptions about the ion-ion potential on the differential cross section of the heavily damped, or deep inelastic, component of heavy ion scattering. Special consideration is given to the angular focussing observed in experiments with heavy projectiles and targets. To obtain focussing at an angle slightly forward of the grazing angle, together with the correct energy loss, a neck degree of freedom for the motion in the exit channel appears necessary. The model is compared with results of scattering experiments of Kr on Bi and Ar on Th, respectively, and is found to reproduce these fairly well.

* Work supported by the U.S. Energy Research and Development Administration, and by the Deutsche Forschungsgemeinschaft.

+ Permanent address: Institut für Kernphysik, Technische Hochschule Darmstadt, Darmstadt, West Germany.

I. INTRODUCTION

The occurence of highly inelastic direct scattering in heavy ion collisions above the Coulomb barrier represents a new and outstanding gross feature of such reactions. When summed over relatively narrow distributions of charge and mass transfers in the reaction products, the deep inelastic events peak at a kinetic energy loss of the order of 100 MeV, well separated from quasi elastic scattering. In some cases also a pronounced peaking in the angular distribution is observed at scattering angles somewhat smaller than the grazing angle [1-5].

It has been pointed out [6] that heavy ion reactions well above the Coulomb barrier can be treated in a classical approximation. In deep inelastic heavy ion scattering, additionally, one sums over a large number of reaction channels, and quantum effects like interference phenomena which still could be present in individual channels disappear completely.

In the classical approximation the scattering cross section $d\sigma/d\Omega$ is derived from the deflection function $\theta(b)$, b being the impact parameter, according to

$$d\sigma/d\Omega = (b/\sin\theta) \cdot |db/d\theta| . \qquad (1)$$

In such a description inelasticity is introduced by assuming, in addition to the conservative Coulomb and nuclear forces, a friction force acting on the relative motion which represents phenomenologivally the transfer of kinetic energy to internal degrees of freedom of the reaction partners, Thus, in terms of ordinary scattering theory one does not follow the motion in the entrance channel, which would be the optical model description, but rather steps through a series of inelastic and reaction channels which have in common that they leave the individuality of projectile and target nearly untouched. It is this situation which is approximated by the classical model.

Heavy ion scattering has been studied in a classical treatment by several authors [7-9]. The models discussed so far are characterized by (i) symmetry between entrance and exit channels, (ii) a rather strong nuclear attraction inside the Coulomb barrier, and (iii) a friction form factor which peaks in the nuclear surface, or even extends [7] to separation distances outside the nuclear interaction region. The deep inelastic events have then to be attributed to forward and "negative angle" scattering, and the cross section rises continuosly to the quasi-elastic peak near the grazing angle. In this form the model does not separate deep inelastic scattering in energy, or angular distribution, from quasi-elastic scattering, contrary to observations.

The model employed here [10] is not intended to give a precision fit to experiments. It rather keeps the kinematics as simple as possible, in order to study the physical implications of several assumptions about the potentials in the entrance and exit channels, and to keep the number of adjustable parameters as small as possible. The model is characterized by three qualitative features which make it different from previous calculations:

(i) The interactions and interaction radii differ in the entrance and exit channels.

(ii) The interaction potential for heavy ions inside the touching radius is shallow due to the strong Coulomb repulsion, and becomes eventually repulsive at distances where nuclear densities would overlap appreciably.

(iii) Energy dissipation is only present in the interaction region. The friction force is exactly zero before touching in the entrance channel, and after scission in the exit channel.

Similar considerations have been put forward recently by Bondorf et al. [11].

II. THE SCATTERING MODEL

For the sake of generating analytically simply soluble equations of motion the potentials V(r) of the conservative forces are either step potentials (at $r = R_i$, or $r = R_c$), or vary as r^{-1} (modified Coulomb potentials), with r being the distance between the centres of gravity of the two fragments. These analytical forms can be easily adjusted to resemble rather closely the real part of various heavy ion potentials (cf. Fig. 4).

The friction is assumed to be purely radial, linear in the velocity, and the corresponding force is

$$F^d(r) = -\lambda(R_t/r)^2(1/c)(dr/dt) \; ; \quad R_t = r_o(A_1^{1/3} + A_2^{1/3}) \qquad (2)$$

in those regions where dissipation is present. The neglect of tangential and rolling friction may be a reasonable approximation during the motion in the entrance channel since in this model no abrupt redistribution of mass is assumed. It is certainly inconsequent for the exit channel in view of the assumption of a neck being built up while the fragments separate. There is, however, not much energy transfer connected with tangential and rolling friction [8]. More important in the previous calculations was the fact that transfer of orbital angular momentum to nuclear rotations opened an important way out of the potential "pocket", leading to substantial changes in the ℓ-dependence of the deep inelastic cross section [8]. This effect has no significance here since the barrier height in the exit channel is already considerably reduced due to the neck elongation.

The choice of the friction form factor $\propto r^{-2}$ is motivated merely by arguments of solubility of the equations of motion. The dominat action of friction is anyhow, through the kinematics, restricted to the regions close to touching and out to scission (cf. Section II).

With these assumptions four radial regions can be defined:

Region I : Entrance channel; $r_{in} > R_i$ (interaction radius)

$V(r) = q^2/r$; $q^2 = Z_1 Z_2 e^2$ (pure Coulomb)

$F^d = 0$

Region II : Entrance channel; $R_i > r_{in} > R_c$ (hard core radius)

$V(r) = f_{ni} q^2/r + c_i$ (modified Coulomb)

$F^d(r) = -\lambda_i (R_t/r)^2 (1/c)(dr/dt)$

Region III : Exit channel; $R_c < r_{out} < R_{sc}$ (scission radius)

$V(r) = f_{no} q^2/r + c_o$ (modified Coulomb)

$F^d(r) = -\lambda_o (R_t/r)^2 (1/c)(dr/dt)$

Region IV : Exit channel; $R_{sc} < r_{out}$

$V(r) = q^2/r$ (pure Coulomb)

$F^d = 0$

The substitution $d\theta = (\ell/\mu r^2).dt$ (θ: angular variable; ℓ: orbital angular momentum, μ: reduced mass) which follows from the integral of the tangential equation (ℓ = const., no tangential friction), and introduction of the new variable $y(\theta) = 1/r(\theta) + \mu f_n q^2/\ell^2$, lead to the radial equation in the form (prime denotes differentiation with respect to θ)

$$y'' - 2\hat{\lambda} y' + y = 0 \; ; \quad \hat{\lambda} = \lambda/(b[8\mu E_{cm}]^{1/2}) \qquad (3)$$

with E_{cm} denoting the centre of mass energy. This equation has solutions in terms of elementary functions.

III. THE ANGULAR FOCUS

Scattering experiments with heavy projectiles, such as Kr, on heavy targets in the lead region [3-5] show a pronounced maximum in the angular distribution at an

angle somewhat smaller than the grazing angle. This angular focus moves together with the grazing angle when the scattering energy is varied [3,4], and consequently can not be attributed to "negative angle" scattering [12].

This section is devoted to some systematic studies of classical trajectories which deviate from Coulomb trajectories under the influence of conservative and non-conservative forces.

At first we study pure potential scattering (without friction), and with no difference in entrance and exit channels. We let the potential be pure Coulomb beyond a certain radius R and ask what radial form has the potential to assume for $r < R$ in order to focus a penetrating beam close to the grazing trajectory at the grazing angle. This question can be studied analytically in terms of a power expansion in a quantity δ which is related to the deviation of the impact parameter b from its value at grazing, b_g.

Introducing dimensionless quantities

$$\varrho = r/R \ , \quad \beta = b/R \ , \quad \varepsilon = E_{cm}/E_c \quad (\text{with } E_c = q^2/R) \tag{4}$$

and defining the trajectory by

$$\nu(\theta) = [\varrho(\theta)]^{-1} - 1 \tag{5}$$

the equation for the trajectory in the Coulomb domain is

$$\nu'' + \nu + 1 = -(1/2\beta^2\varepsilon) \ . \tag{6}$$

With the correct asymptotic boundary conditions the solution of Equ. (6) is

$$\nu(\theta) = (1/2\beta^2\varepsilon)\left[\sqrt{1 + (2\beta\varepsilon)^2}\cos(\theta - \theta') - (1 + 2\beta^2\varepsilon)\right] \tag{7}$$

for $\theta \geq \theta_I$. The Coulomb turning angle θ' is given by

$$\theta' = \pi - \text{arctg}(2\beta\varepsilon) \ , \tag{8}$$

and the interaction angle (for which $\nu = 0$) by

$$\theta_I = \theta' + \arccos((1 + 2\beta^2\varepsilon)/\sqrt{1 + (2\beta\varepsilon)^2}) \ . \tag{9}$$

The grazing orbit is defined by

$$\beta_g = \sqrt{(\varepsilon - 1)/\varepsilon} \quad ; \quad \theta'_g = \pi - \operatorname{arctg}(2\sqrt{\varepsilon(\varepsilon - 1)}) . \tag{10}$$

Defining the expansion parameter

$$\delta = \beta_g \sqrt{1 - (\beta/\beta_g)^2} > 0 ; \quad \delta \ll 1 \tag{11}$$

and the new variable

$$\phi = \theta - \theta'_g \quad ; \quad \phi \ll 1 \tag{12}$$

one can expand the solution for $\theta > \theta_I$ up to second order in δ and ϕ.

For $\varrho \leq 1$ we make an ansatz for the solution

$$\nu(\phi) = a_o + a_2\phi^2 + a_4\phi^4 \quad ; \quad \theta \lesssim \theta_I . \tag{13}$$

Taking only even powers in ϕ renders the solution symmetric with respect to $\phi = 0$ ($\theta = \theta'_g$) and focusses the outgoing trajectories automatically at the grazing angle $\theta_g = 2\theta'_g - \pi$.

The boundary conditions at $\phi = \phi_I$

$$\nu(\phi_I) = 0 \quad \text{and} \quad \nu'(\phi_I^+) = \nu'(\phi_I^-) \tag{14}$$

determine a_o and a_2 while a_4 is fixed through the differential equation

$$\nu'' + \nu + 1 = -(1/2\beta^2 \varepsilon q^2)(F(\nu)/(1 + \nu)^2) \quad ; \quad \theta \lesssim \theta_I \tag{15}$$

by demanding the force $F(\nu)$ to be independent of ϕ. It is the second derivative in the differential equation (15) which makes it necessary to include a fourth order term in Equ. (13) for a consistent expansion up to second order in δ and ϕ.

The potential of the purely radial force which leads to the solution Equ. (13) of Equs. (14) and (15) is given by

$$V(\varrho) = (q^2/R)\left\{ [1 + g(\varepsilon)]\frac{1}{\varrho} - \frac{1}{2} g(\varepsilon)\frac{1}{\varrho^2} - \frac{1}{2} g(\varepsilon) \right\} ; \quad \varrho \leq 1 \tag{16}$$

with

$$g(\varepsilon) = \frac{2\varepsilon(\varepsilon - 1) + 1}{\varepsilon - 1} \tag{17}$$

The function $g(\varepsilon)$ is plotted in Fig. 1a. The larger $g(\varepsilon)$ the more the potential deviates from its pure Coulomb form $\propto \varrho^{-1}$ in the region $\varrho < 1$. The minimum value

of $g(\varepsilon)$ is $g(\underline{\varepsilon}) \simeq 4.83$ for $\varepsilon \simeq 1.71$.

Fig. 1b shows the focussing potentials, normalized to the Coulomb barrier at $\varrho = 1$, for various values of ε, the scattering energy in units of the Coulomb barrier. The potentials for $\varepsilon = 1.5$ and $\varepsilon = 2$ are the same as can be seen from Fig. 1a. The flattening of the focussing potential in the region where the expansion is valid becomes more pronounced if ε increases beyond the minimum value $\underline{\varepsilon} = 1.71$.

Next we use the model set up in the previous section for a systematic study of the effect of some major ingredients of heavy ion dynamics on the classical trajectories.

Since the combined nuclear and Coulomb interactions for very heavy ion scattering lead to a potential which is nearly flat inside the touching point of the two nuclei, becoming repulsive again for still smaller distances, we use as a starting point a constant potential for distances smaller than touching ($r < R_i$), being matched to a pure Coulomb potential outside ($r > R_i$). In a constant potential the trajectories are straight lines which leads already to an approximate forward focus at positive scattering angles (cf. Fig. 2a). This argument would apply as well to a quantum mechanical treatment since in a force-free region the phase relations for different partial waves are such as to focus the total wave at forward scattering.

Deviations of the potential from its constant value inside the interaction region are generated by (i) a discontinuity ΔV at the interaction radius $\varrho = 1$, representing a "pocket" in the potential, (ii) a scission radius ϱ_{sc} differing from $\varrho = 1$ in the exit channel, simulating a "neck" in that channel, and (iii) a friction-force of the form Equ. (2) in the interaction region $\varrho < 1$ and $\varrho < \varrho_{sc}$, respectively. The general potential obtained in this way is sketched in Fig. 2.

Fig. 3 shows the classical trajectories for a bundle of impact parameters, starting with the flat potential and successively switching on the neck, the pocket,

and friction, or combinations of these. As can be seen from the series of pictures, only when a neck avoids for the outgoing trajectories the high Coulomb barrier of the entrance channel is the friction force able to preserve a focus at positive scattering angles (Figs. 3f and g). The pocket, or net attraction, of the potential then merely changes the focussing angle relative to the grazing angle. The values taken for Δv, ρ_{sc}, $\mathcal{E}$, and for the friction force constant λ, are close to the realistic values for a typical heavy ion scattering situation such as Kr on Bi, as derived for this case in Section IV (cf. also Table 1).

As can be seen from Figs. 3f and g, the focussed trajectories have almost equal path length in the interaction region, leading to a roughly constant energy loss for the focussed bundle of impact parameters. It should be noted that the energy loss in the situation of Fig. 1d for the same value of the friction constant is very small for the beams which are scattered to positive angles, while increasing the friction constant would bend these trajectories over to negative scattering angles.

IV. APPLICATION TO HEAVY ION SCATTERING

In this section we adjust the model to realistic heavy ion scattering situations in order to see if the characteristic experimental observations, the energy loss and the differential cross section of the heavily damped component, as well as their variations with bombarding energy and projectile-target composition can be quantitatively reproduced.

There are two derivations of ion-ion potentials from assumptions about nuclear interactions which represent opposite limiting cases of the situation to be expected in heavy ion collisions. One is the adiabatic ion-ion potential of Nix and collaborators [13], assuming at each step a complete relaxation of nuclear densities into a neck degree of freedom. The other is the proximity force potantial of Randrup, Swiatecki and Tsang [14] which assumes frozen densities of the two nuclei, and conse-

quently contains a strong repulsion in the density overlap region.

For the entrance channel the parameters of the model, R_i, R_c, f_{ni}, c_i, are fixed so as to reproduce as closely as possible either the adiabatic ion-ion, or the proximity force potentials (cf. Fig. 4). Firstly, the core radius is chosen such as to place the radial $\ell = 0$ turning point into a region where the potential to be reproduced becomes strongly repulsive. Then the modified Coulomb potential is smoothed to the actual potential in the region $R_i > r_{in} > R_c$. For the adiabatic potential the core radius is irrelevant (and has been chosen only for calculational purposes) since the angular momentum barrier cuts out the relative motion from distances $\lesssim 8$ fm (in the Kr,Bi case) for all trajectories which are not absorbed ($\ell \gtrsim 21\hbar$). For the actual calculation of the adiabatic potential an extrapolation of the potential constants to asymmetric systems proposed by Krappe and Nix [15] has been used. Within the limits of accuracy, whose influence on the results have been checked and found to be small, the model potentials of the entrance channel contain no free parameters.

For the exit channel, according to assumption (i) of section I, the buildup of a neck is assumed before the two nuclei separate. For the determination of the scission point R_{sc} the following procedure has been adopted. Blocki and Swiatecki [16] have calculated liquid drop potential energies for two interpenetrating nuclei, depending on two parameters, their relative distance, and the amount of matter which is transferred into a neck resulting from joining the two nuclei smoothely with a second order surface. In the corresponding two-dimansional plot of the potential energy surface a starting point is chosen which corresponds to the classical turning point in the relative motion. Then a path of steepest descent is followed out to the point where scission occurs, and the corresponding relative distance of the fragments

is taken as the scission radius R_{sc}. Since no inertial parameters are known along this path the scission point can be determined only approximately by this procedure. The results, however, do not depend very critically on R_{sc}, as long as it is considerably larger than the interaction radius R_i. The potential in the exit channel region III is then uniquely determined by matching the entrance channel potential at the classical turning point, and reaching the Coulomb barrier of the outgoing particles at the scission point.

The friction force constants λ_i, λ_o are treated as free parameters. Since only the total energy loss of the highly damped component is known experimentally, and since no significant change of the deflection function resulted from varying λ_i and λ_o independently within reasonable limits, $\lambda_i = \lambda_o$ has been chosen, and this friction constant was adjusted to give the correct order of magnitude for the observed inelasticity. The potential parameters derived in this way are listed in Table 1.

The deep inelastic collisions studied are taken from the work of Artukh et al.[1], Hanappe et al.[3], and Wolf et al.[4] which refers to the systems $^{40}Ar + ^{232}Th$ and $^{84}Kr + ^{209}Bi$, respectively. Fig. 4 shows the proximity force and adiabatic ion-ion potentials together with the Coulomb repulsion for the system Kr + Bi, and the correspondingly adjusted model potentials. Fig. 5 gives the deflection functions (a) without friction, and (b) for the chosen value of the friction force constant (cf. Table 1). As can be read off from the deflection functions, the model potential resembling the adiabatic ion-ion potential leads to absorption ("fusion") for the low ℓ-values with $\ell_{crit} \simeq 21\,\hbar$ (corresponding to $\sigma_{abs} \simeq 12$ mb). The deflection function of the model potential close to the proximity force looks considerably different. It does not lead to absorption because of the small nuclear interpenetration caused by the repulsive core of that potential. Both model potentials lead to angular focussing, indicated by the flattened parts of the deflection functions in the ℓ-range $80 \lesssim \ell/\hbar \lesssim 150$. The experimantal angular distributions of the deep inelastic compo-

nent, however, are better reproduced if the proximity-like potential is used in the entrance channel. For this reason, only the results for the proximity force model potential are shown in the figures giving the cross sections. The qualitative results for both potentials are, however, quite similar, and it would be interesting to perform a dynamic calculation in an extended space in order to see to what extent the frozen density situation relaxes into collective degrees of freedom.

The distances of closest approach for the larger of the two energies (system Kr + Bi) are r_{min} = 10 fm (proximity force), and r_{min} = 8 fm (adiabatic potential). In the case of the adiabatic potential where absorption takes place for the low impact parameters this refers to the first trajactory which scatters again out of the interaction region.

Fig. 6 shows the differential cross section (proximity force model potential in the entrance channel) in comparison with experimental results. The classical cross section has a rather sharp edge towards lower angles. This would be changed in a quantum mechanical calculation allowing for barrier penetration. The comparison shows that the location of the angular focus and the order of magnitude of the deep inelastic cross section are given correctly by the model, for both energies in the system Kr on Bi. In the scattering of Ar on Th, however, the observed continous rise of the angular distribution towards lower angles is not reproduced. The figure also indicates the centre-of-mass energies of the outgoing particles, and their variations over the angular peak. This variation agrees qualitatively with a plot of the double-differential cross section $d^2\sigma/dEd\theta$ of the heavily damped component, extracted from the experimental results [17].

V. CONCLUSION

The model calculation reported here gives evidence that the observed angular distribution of the heavily damped component in heavy ion scattering is connected to (i) a nearly flat region in the summed nuclear and Coulomb ion-ion interactions, and (ii) the occurence of a neck in the exit channel allowing for relaxation of a large amount of the kinetic energy into internal excitations before scission. Only both effects together result in the narrow energy distribution scattered into a narrow angular range, as observed experimentally. Adiabacity with respect to the neck degree of freedom is reached only gradually during the time of strong interaction, as is indicated by the very low fusion cross sections of the heavy scattering systems which is better described in terms of the "frozen density" proximity force.

It is a pleasure to acknowledge stimulating discussions with W. D. Myers, W. J. Swiatecki, and C. F. Tsang, as well as to thank N. K. Glendenning and the Nuclear Theory Group of the Lawrence Berkeley Laboratory for their hospitality.

REFERENCES

1) A. G. Artukh, G. F. Gridnev, V. L. Mikheev, V. V. Volkov, and J. Wilczynski, Nucl. Phys. A215, 91 (1973).

2) M. Lefort, C. Ngo, J. Peter, and B. Tamain, Nucl. Phys. A216, 166 (1973).

3) F. Hanappe, M. Lefort, C. Ngo, J. Peter, and B. Tamain, Phys. Rev. Lett. 32, 738 (1974); Proc. Nashville Conference on Reactions Between Complex Nuclei, North-Holland Publishing Company, Vol. 1, 116 (1974).

4) K. L. Wolf, J. P. Unik, J. R. Huizenga, J. Birkelund, H. Freiesleben, and V. E. Viola, Phys. Rev. Lett. 33, 1105 (1974).

5) L. Moretto, private communication.

6) Cf. e.g. R. A. Broglia and A. Winther, Physics Reports 4, 153 (1972).

7) D. H. E. Gross and H. Kalinowski, Phys. Lett. 48B, 302 (1974).

8) J. P. Bondorf, M. I. Sobel, and D. Sperber, Physics Reports 15, 83 (1974).

9) C. F. Tsang, LBL Report 2928 (1974).

10) F. Beck, Proc. International Workshop on Gross Properties of Nuclei and Nuclear Excitations III, Hirschegg, AED-Conf-75-009-000, 135 (1975).

11) J. P. Bondorf, J. R. Huizenga, M. I. Sobel, and D. Sperber, Phys. Rev. C11, 1265 (1975).

12) This important consequence was pointed out to the author by W. D. Myers, private communication.

13) J. R. Nix and A. J. Sierk, Los Alamos Preprint LA-UR-74-880 (1974).

14) J. Randrup, W. J. Swiatecki, and C. F. Tsang, LBL Report 3603 (1974).

15) H. J. Krappe and J. R. Nix, Proc. Third IAEC Symposion on Physics and Chemistry of Fission, Rochester 1973, IAEA Vienna, Vol. I, 159 (1974), and J. R. Nix, private communication.

16) J. Blocki and W. J. Swiatecki, Nuclear Chemistry Annual Report 1974, LBL-4000, and private communication.

17) K. L. Wolf and C. F. Tsang, private communication.

Table 1

Potential and friction force parameters for the results given explicitly in the text

	R_i (fm)	R_c (fm)	f_{ni}	c_i (MeV)	λ_i[a] (MeV/fm)	R_{sc} (fm)	f_{no}	c_o (MeV)	λ_o[a] MeV/fm)
				$^{84}Kr + ^{209}Bi$					
Proximity force potential	13.0	10.0	0.4	176.7	420.3	22.0	0.6	67.1	420.3
Adiabatic ion-ion potential	13.5	0.5	-6.10^{-3}	320.9	420.3	22.0	9.10^{-3}	194.1	420.3
				$^{40}Ar + ^{232}Th$					
Proximity force potential	12.0	8.0	0.9	-10.0	184.4	25.2	0.8	14.8	184.4

[a] r_o used in the definition of the friction force, equ. (2), r_o = 1.22 fm

FIGURE CAPTIONS

Fig. 1. (a) The function $g(\varepsilon)$ which determines the deviation of the focussing potential from the Coulomb form. ε is the scattering energy in units of the Coulomb barrier energy $E_c = Z_1 Z_2 e^2/R$.

(b) The reduced scattering potential $V(r/R)/V(1)$ which leads to a focus at the grazing angle, and its dependence on the scattering energy ε. The hatched bar on the potential curves indicates the penetration depth at which corrections to the expansion reach the order of 20 %.

Fig. 2. The reduced model potentials $v(\rho) = V(\rho)/V(1)$ in the entrance (in) and exit (out) channels as functions of $\rho = r/R$. ρ_t is the classical turning point at which the in- and out-potentials are matched to be equal.

Fig. 3. Series of scattering trajectories for various model potentials and reduced impact parameters $\beta = 0.23$, 0.45, 0.68, and 0.91, respectively.

(a) Flat potential, $\Delta v = 0$, $\rho_{sc} = 1$.

(b) Flat potential + neck, $\Delta v = 0$, $\rho_{sc} = 1.69$.

(c) Flat potential + pocket, $\Delta v = 0.15$, $\rho_{sc} = 1$.

(d) Flat potential + friction, $\Delta v = 0$, $\rho_{sc} = 1$, $\lambda \cdot R/E_c = 16.5$.

(e) Flat potential + pocket + neck, $\Delta v = 0.15$, $\rho_{sc} = 1.69$.

(f) Flat potential + neck + friction, $\Delta v = 0$, $\rho_{sc} = 1.69$, $\lambda \cdot R/E_c = 16.5$.

(g) Flat potential + pocket + neck + friction, $\Delta v = 0.15$, $\rho_{sc} = 1.69$, $\lambda \cdot R/E_c = 16.5$.

All trajectories are for scattering energies $\varepsilon = 1.13$.

Fig. 4. (a) Sum of the proximity force (approximation A of ref. 14) and Coulomb potentials for the system $^{84}Kr + ^{209}Bi$ (solid line), and model potential approximation to this potential (broken line). The two c.m.energies for

which calculations have been performed are also indicated.

(b) The same as (a) for the adiabatic ion-ion potential of ref. 13,15.

Fig. 5. (a) Deflection function for $^{84}Kr + ^{209}Bi$ calculated for the model potential resembling the proximity force. The c.m.energy is 374 MeV. a) no friction case, b) friction force constant as in Table 1.

(b) The same as (a) with the model potential for the adiabatic ion-ion force.

Fig. 6. (a) Calculated cross section (proximity force model potential) for the deep inelastic component in the scattering of ^{84}Kr on ^{209}Bi (solid lines), together with the experimental results of ref. 3 and 4 (dot-dashed lines). a) refers to 374 MeV (right scale), and b) to 428 MeV (left scale) c.m.energies.

(b) Calculated cross section (proximity force model potential) for ^{40}Ar on ^{232}Th at 331 MeV c.m.energy (solid line). For comparison, selected reaction product yields as given in ref. 1 are shown (dot-dashed lines).

The variation of the outgoing (inelastic) c.m.energies is indicated by the figures (which are in MeV) along the cross section curves. The friction force constants are as given in Table 1.

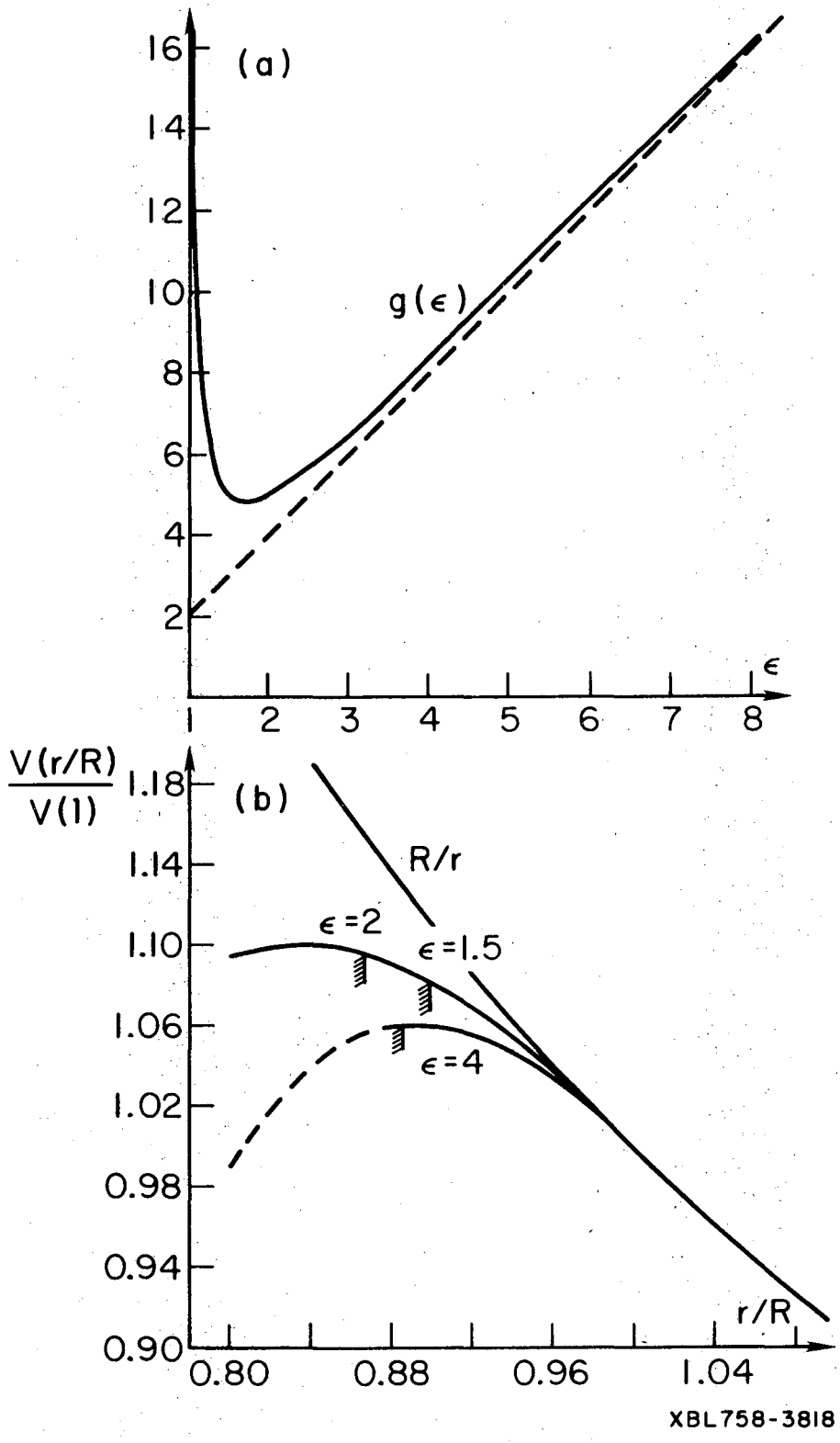
(a)
16
14
12
10
8
6
4
2
g(ϵ)
ϵ
1
2
3
4
5
6
7
8
V(r/R)
V(1)
(b)
1.18
1.14
1.10
1.06
1.02
0.98
0.94
0.90
R/r
ϵ=2
ϵ=1.5
ϵ=4
r/R
0.80
0.88
0.96
1.04
XBL758-3818

Fig. 1

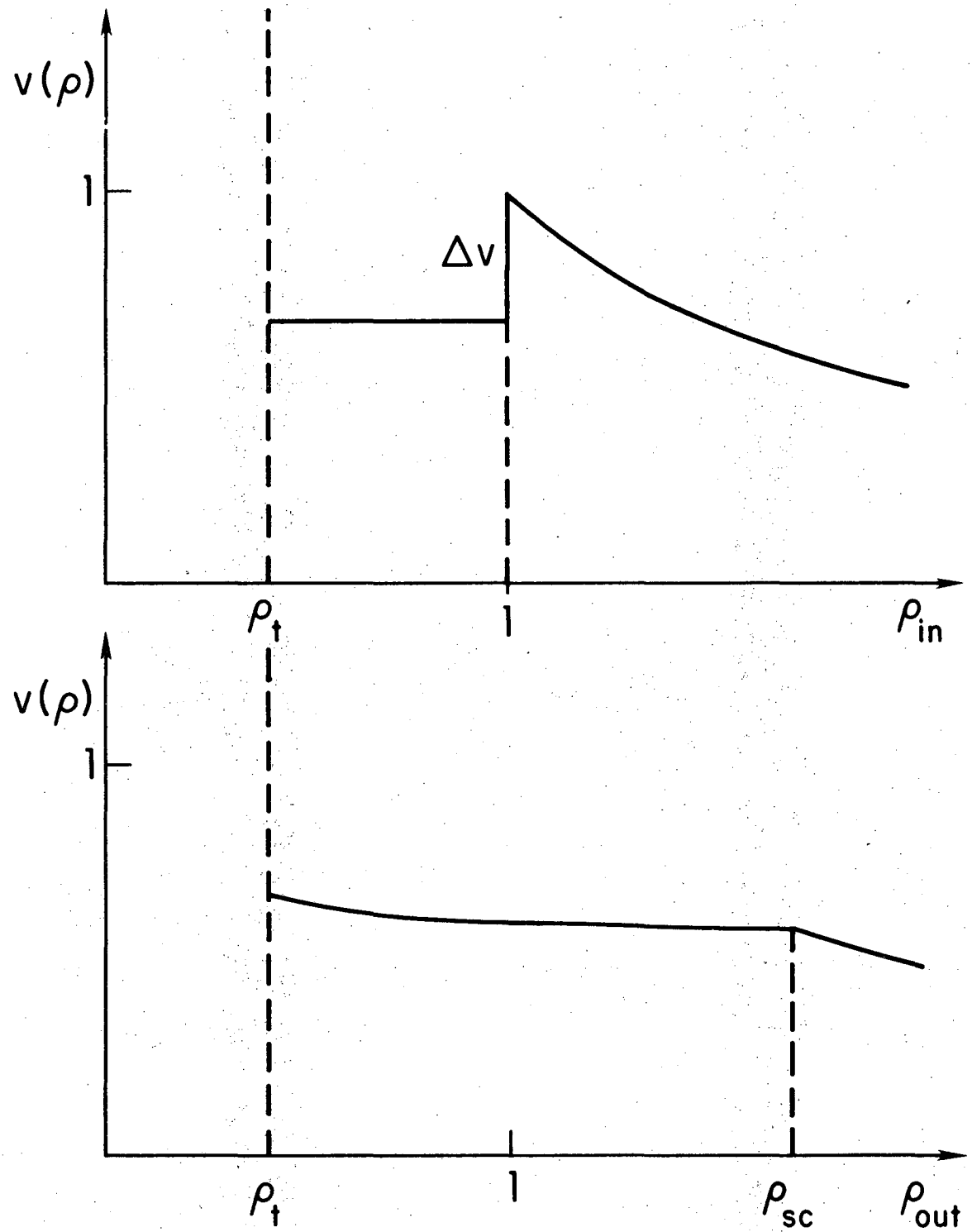

Fig. 2

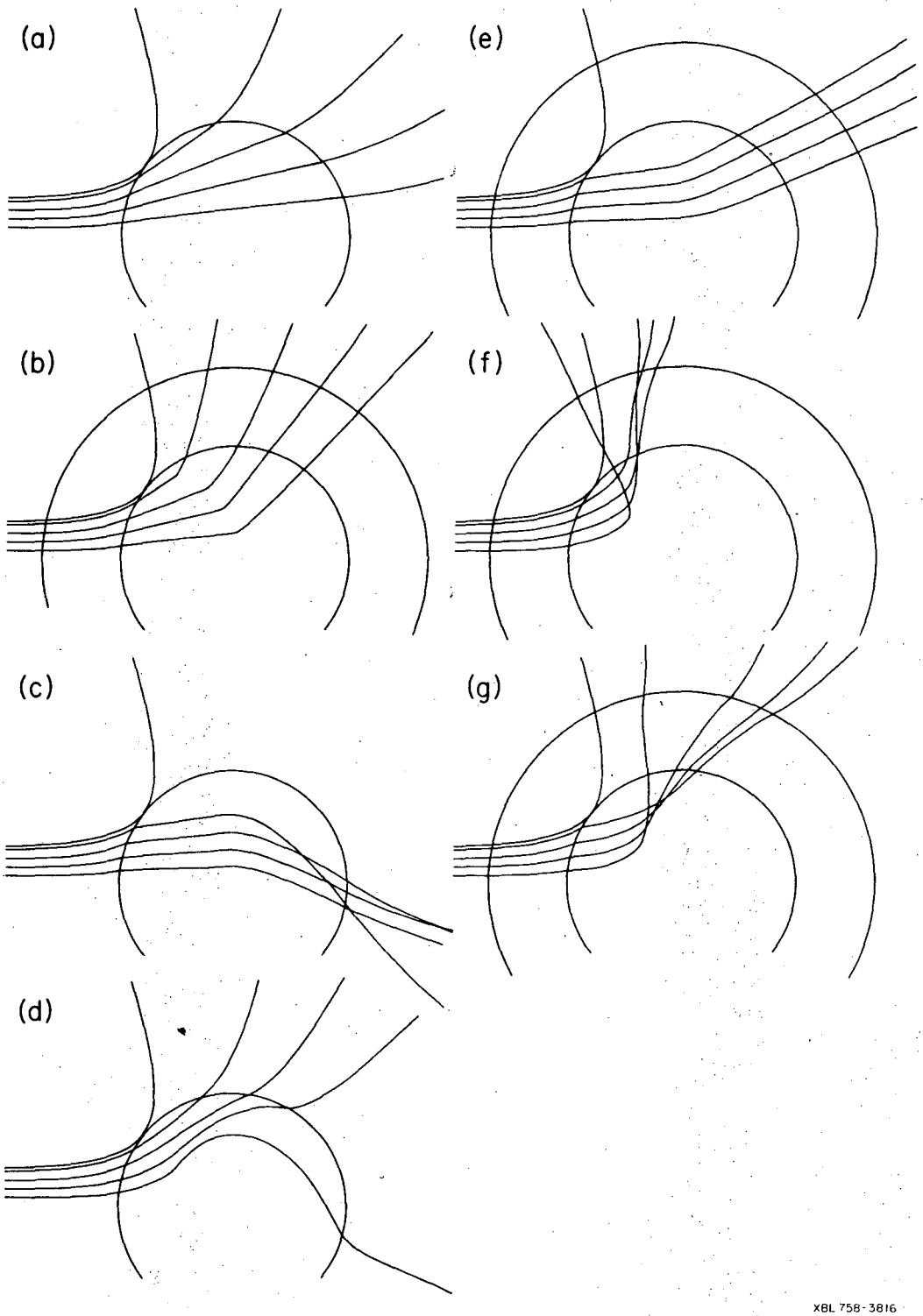

Fig. 3

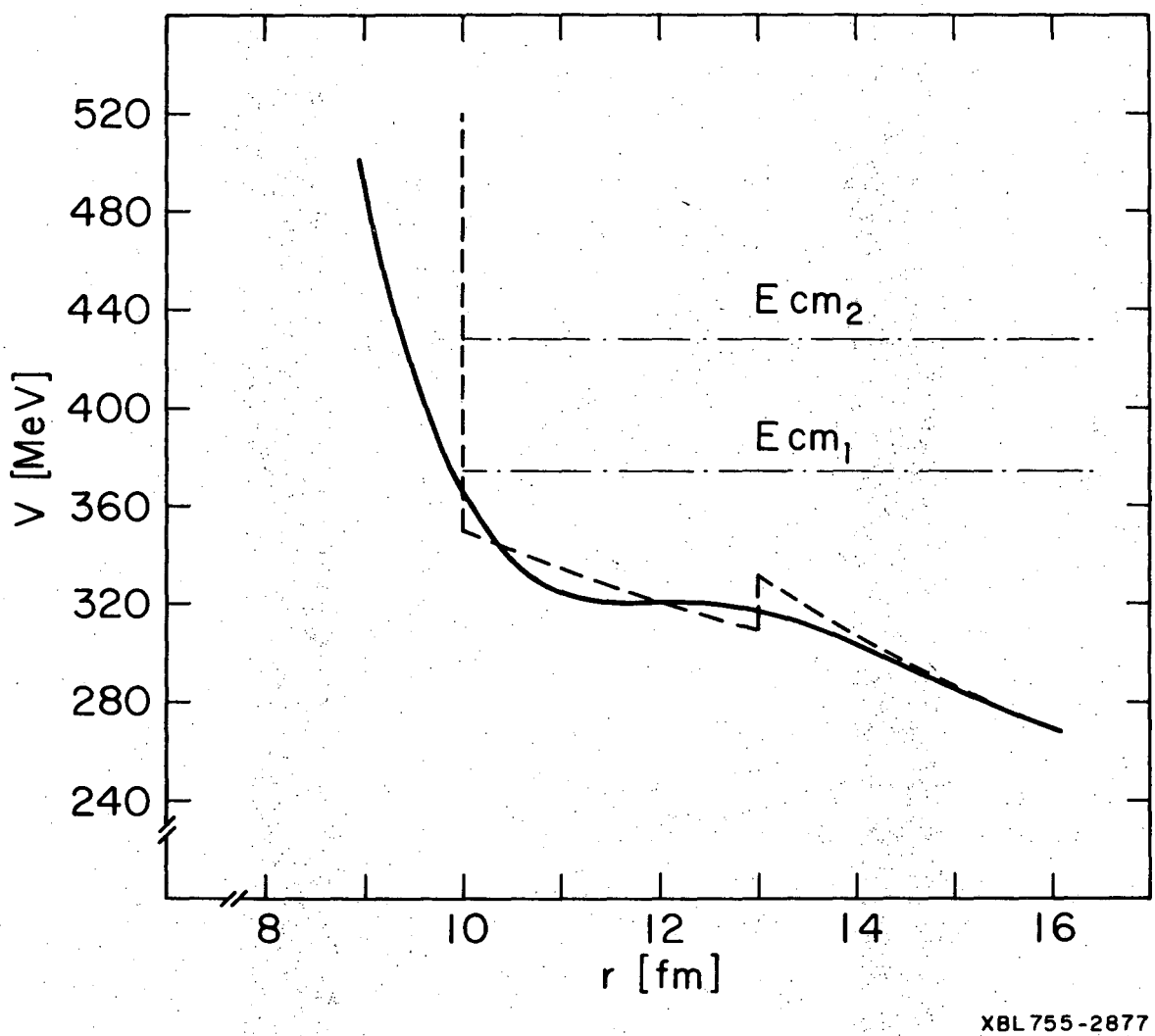
520
480
440
400
360
320
280
240
V [MeV]
E cm2
E cm1
8
10
12
14
16
r [fm]
XBL755-2877

Fig. 4a

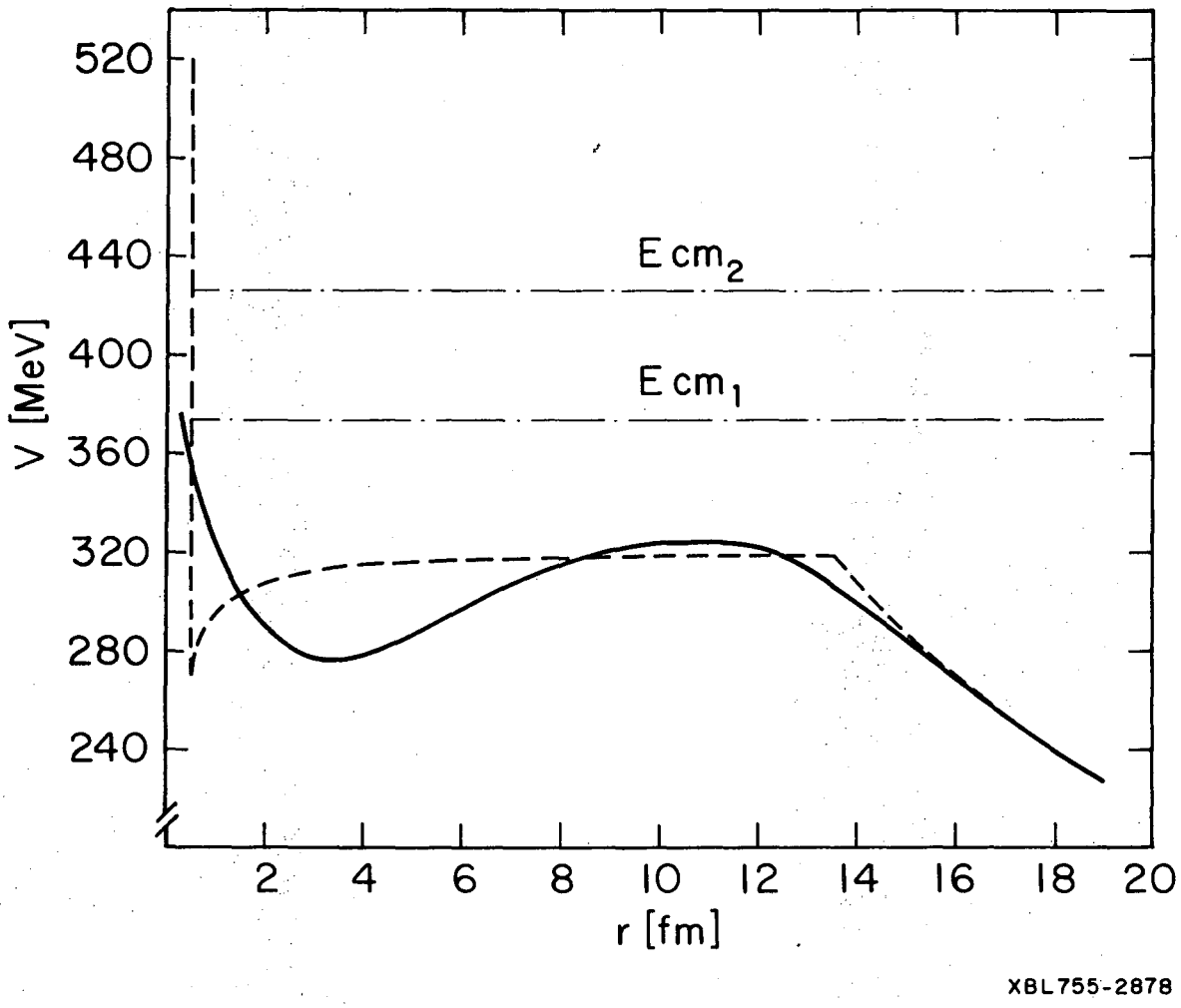

Fig. 4b

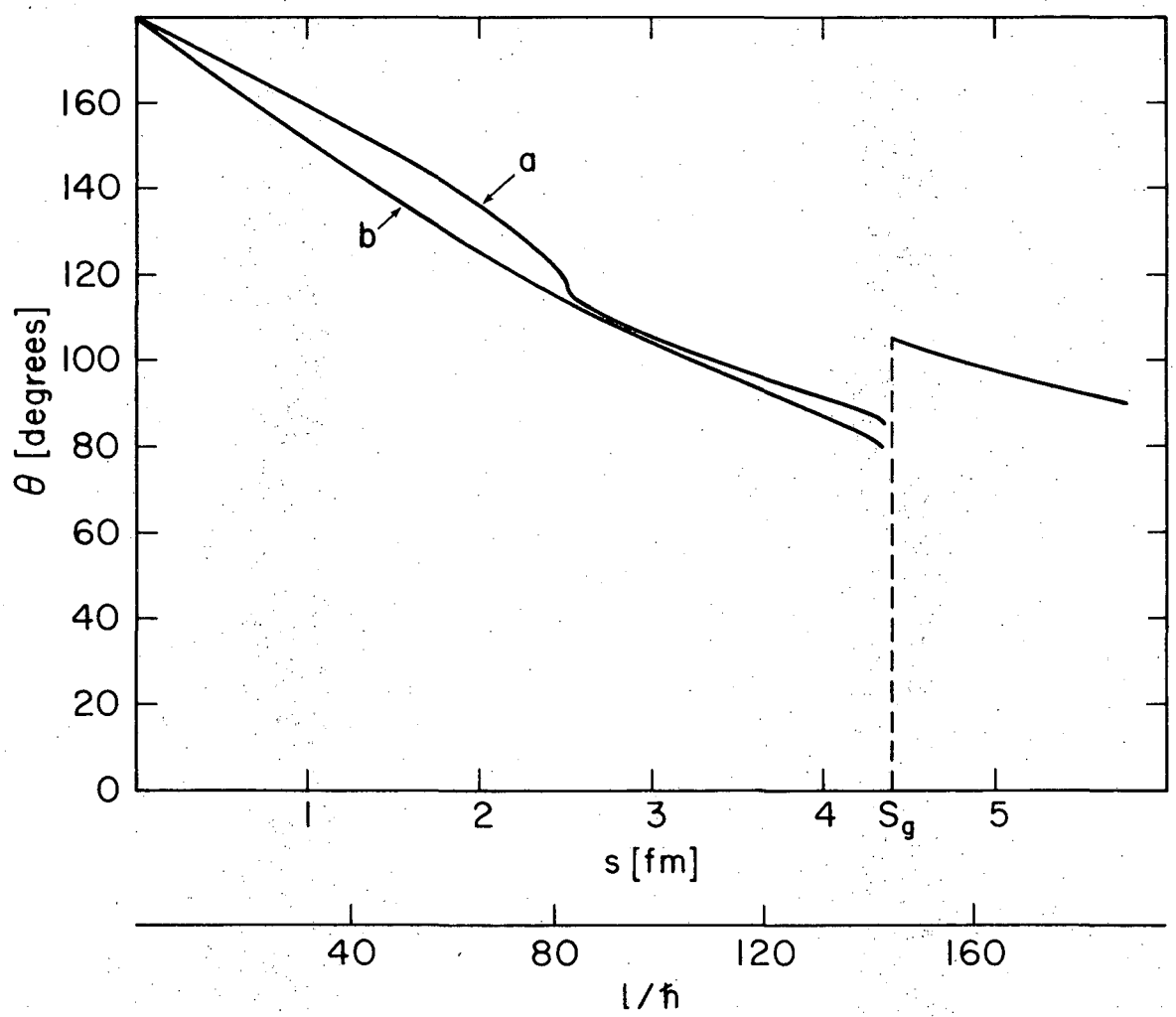
160
140
120
100
80
60
40
20
0
θ [degrees]
a
b
1
2
3
4
S_g
5
s [fm]
40
80
120
160
l/ħ
XBL 755-2879

Fig. 5a

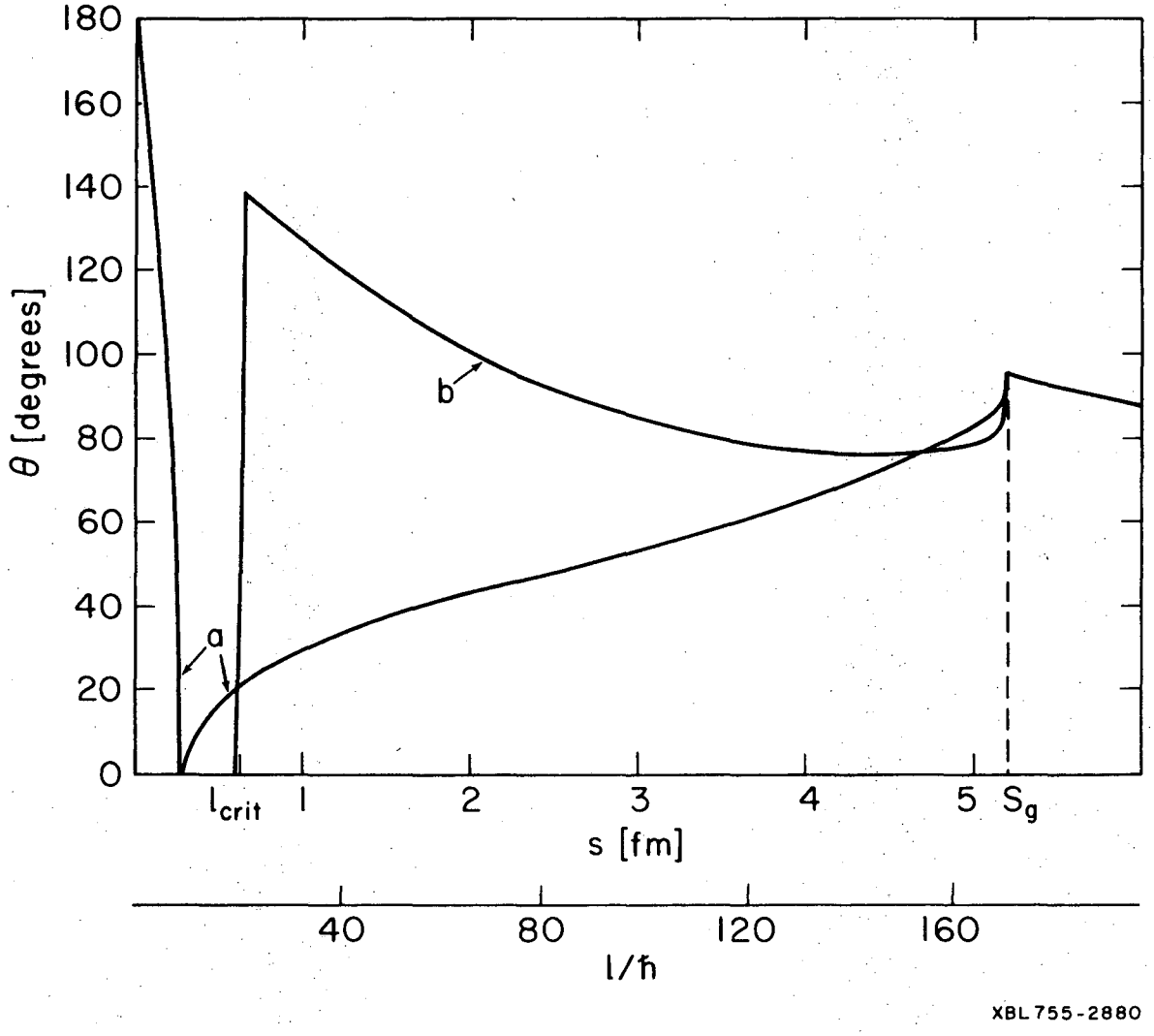

Fig. 5b

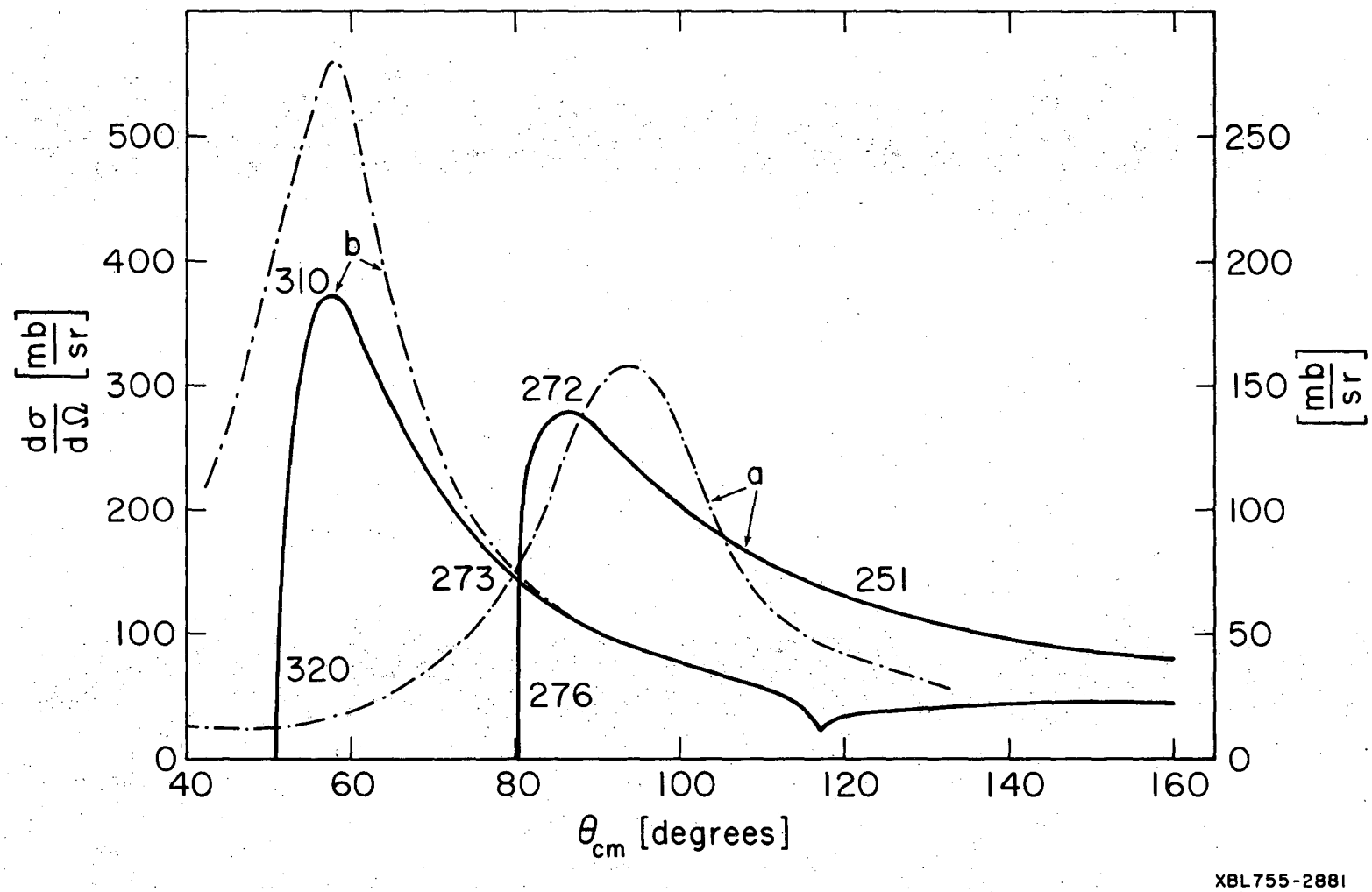
500
400
300
200
100
0
250
200
150
100
50
0
40
60
80
100
120
140
160
$\frac{d\sigma}{d\Omega}$ [mb/sr]
[mb/sr]
θ_{cm} [degrees]
310
b
272
a
273
251
320
276
XBL755-2881

Fig. 6a

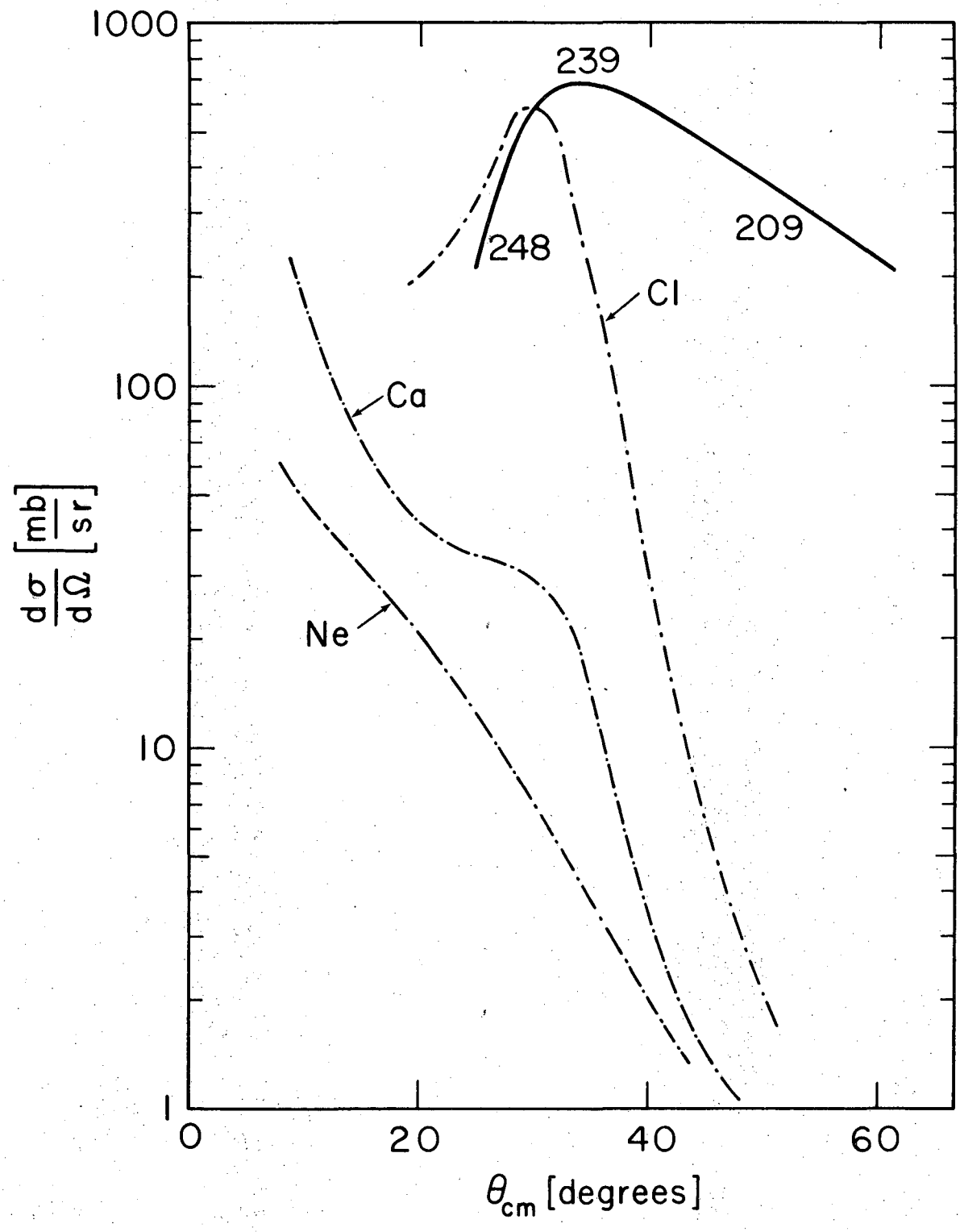
1000
100
10
1
239
248
209
Cl
Ca
Ne
$\frac{d\sigma}{d\Omega}\left[\frac{mb}{sr}\right]$
0
20
40
60
θ_{cm} [degrees]
XBL 755-2882

Fig. 6b

TECHNICAL INFORMATION DIVISION
LAWRENCE BERKELEY LABORATORY
UNIVERSITY OF CALIFORNIA
BERKELEY, CALIFORNIA 94720